THE JOURNAL OF PHYSICAL CHEMISTRY C

Article

pubs.acs.org/JPCC

Temperature Dependence of Electron–Phonon Interactions in Gold Films Rationalized by Time-Domain Ab Initio Analysis

Xin Zhou,[†,‡] Linqiu Li,[‡] Hao Dong,[‡,§] Ashutosh Giri,[∥] Patrick E. Hopkins,[∥,⊥,@] and Oleg V. Prezhdo*[,‡,▽]

[†]College of Environment and Chemical Engineering, Dalian University, Dalian 116622, P. R. China

[‡]Department of Chemistry, University of Southern California, Los Angeles, California 90089, United States

[§]Institute of Chemistry for Functionalized Materials, School of Chemistry and Chemical Engineering, Liaoning Normal University, Dalian, Liaoning 116029, P. R. China

[∥]Department of Mechanical and Aerospace Engineering, University of Virginia, Charlottesville, Virginia 22904, United States

[⊥]Department of Materials Science and Engineering, University of Virginia, Charlottesville, Virginia 22904, United States

[@]Department of Physics, University of Virginia, Charlottesville, Virginia 22904, United States

[▽]Department of Physics and Astronomy, University of Southern California, Los Angeles, California 90089, United States

ABSTRACT: The nonequilibrium dynamics of excited electrons in metals is probed by ultrafast laser measurements. Using a real-time Kohn–Sham time-dependent density functional theory and nonadiabatic molecular dynamics, we report direct modeling of such experiments, rationalizing the observed temperature dependence. Focusing on thin gold films, we analyze the effect of temperature on film structure, electronic state densities, nonadiabatic electron–phonon coupling, elastic electron–phonon scattering times, and electron–phonon relaxation rates. The effective electron–phonon coupling constants calculated at different temperatures are in good agreement with the values deduced from experiments and an alternative theory. A temperature increase accelerates both inelastic and elastic electron–phonon scattering and allows a larger number of higher-frequency phonon modes to couple to the electronic subsystem. The inelastic electron–phonon coupling is largest between nearest states, indicating that carrier relaxation involves transitions over small energy increments. In contrast, the elastic electron–phonon scattering is strongest for pairs of electronic states that are distant in energy. The electron–phonon interactions exhibit mild energy dependence, with both nonadiabatic electron–phonon coupling and elastic electron–phonon scattering times decreasing with increasing electron excitation energy. The detailed ab initio analysis of the electron–phonon interactions emphasizes the nonequilibrium nature of the relaxation processes and provides important insights into the electron–phonon energy exchange in metal films in general.

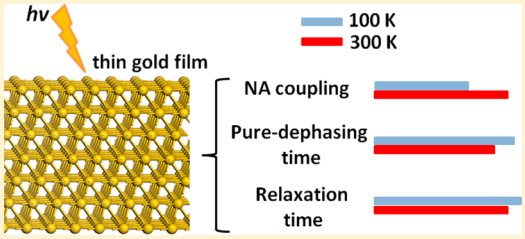

1. INTRODUCTION

A thorough understanding of electron–phonon scattering processes taking place during thermal equilibration of excited electrons with the lattice is critical for a wide array of applications.[1−12] Taking place on pico- and subpicosecond time scales, the processes are most directly observed using time-resolved pump–probe laser techniques.[13−37] Irradiation of a metal film or a nanostructure with an ultrashort laser pulse drives the electron gas out of thermodynamic equilibrium,[38] and subsequent electron–phonon interactions can lead to melting, ablation, and spallation.[9,11,12,39] The rate of electronic relaxation during and after the pulse absorption dictates the evolution of the effective electron and phonon temperatures, with the electron–phonon coupling providing an essential pathway of conversion of photonic energy into heat.

Eesley first observed the nonequilibrium between the electronic and vibrational states in metals with short-pulsed, time-domain thermo-reflectance (TDTR) spectroscopy, which confirmed the earlier two-temperature model theory.[38,40−42] In this model, the electrons are taken to have a Fermi–Dirac distribution with temperature T_e, and the phonons have a Planck distribution with temperature T_l. Energy transfer between the electron and phonon subsystems makes T_e and T_l eventually equal. Later, femtosecond laser pulses were used to resolve the time taken by the electronic system to lose its energy to the lattice, allowing for the measurement of the electron–phonon coupling constant, G, that quantifies the volumetric rate of energy transfer between the two subsystems.[15,43−46] Still, several critical questions on the fundamental scattering processes driving this energy transport remain unanswered. For example, what processes contribute most significantly to the overall rate of energy transfer from an excited electron system to the lattice: electron–electron scattering or electron–phonon scattering? How do the nonthermal versus thermal states of the electron and phonon systems affect electron–phonon equilibration? Several works

Received: May 29, 2017
Revised: July 16, 2017
Published: July 24, 2017

DOI: 10.1021/acs.jpcc.7b05211
J. Phys. Chem. C 2017, 121, 17488−17497

have attempted to answer these questions through extensive predictive modeling;[24,29,47−56] these works have relied on theoretical, semiclassical (Boltzmann transport equation-based), classical (atomistic), or some combination of the approaches. However, to the best of our knowledge, a rigorous treatment of this problem that quantum mechanically describes the nonequilibrium electronic system from first-principles while atomistically accounting for the lattice energies and vibrations has not been undertaken. Hence, the assumptions that have been invoked in these previous treatments of this problem have left the aforementioned questions unanswered, leading to a void in our understanding of the interplay among the phase space of electron, phonon, thermal, and nonthermal, coupling mechanisms.

For example, from free electron theory, Chen et al.[47] proposed a linear change in the effective electron−phonon coupling, G_{eff}, with the electron and phonon temperatures. The model is only valid for free electron metals with a relatively constant density of states (DOS) and assumes the DOS is constant over all electron temperatures (up to the Fermi temperature). Lin et al.[54] studied the temperature dependence of the electron−phonon coupling factor for several metals using an ab initio DOS for electrons based on Allen's theoretical investigation.[2] This work demonstrated that electronic states several electronvolts below the Fermi energy can have a pronounced effect on G due to thermal excitations, showing that the assumption of a constant DOS can be invalidated at electron temperatures typical in TDTR experiments (>10^3 K), even in free electron metals. Their theory only treats the electron−phonon scattering problem and assumes that the electrons can be described by a Fermi distribution. Furthermore, this work does not take into account nonthermal electron-to-phonon coupling or electron−electron scattering on the overall rate of electron−phonon relaxation. Mueller and Rethfeld[55,56] extended on Lin et al.'s investigation by accounting for electron−electron scattering and nonthermal distributions through a Boltzmann Transport Equation approach applied to the electrons, the DOS of which were determined via ab initio techniques. Recently, Giri and Hopkins[48] used a purely analytical approach to account for nonthermal electron dynamics and electron−electron scattering in G to recreate transient relaxation data typically observed in TDTR experiments.

Recently, Hopkins and co-workers used TDTR to establish that electron−electron scattering in Au films can enhance the effective rate of electron−phonon relaxation when the electrons are highly out of equilibrium with the surrounding lattice.[21,37,57] They demonstrated experimentally that the electron−phonon coupling factor in gold increases with increasing lattice temperature and absorbed laser fluences and that at relatively low laser fluences, the energy relaxation between electrons and phonons is mainly governed by the nonthermal distribution of electrons.[21] They also found that electron−electron scattering along with electron−phonon scattering have to be considered simultaneously to correctly predict the transient nature of electronic relaxation after short-pulsed laser heating of metals at elevated electron temperatures.[48] To properly account for the electron and phonon dynamics in these experiments and to offer the ability to extend predictions to a wide variety of systems, first-principles quantum mechanical simulation approaches should be invoked. The approaches should properly account for the excited electron dynamics and electron−phonon relaxation typical in short-pulsed, pump−probe laser experiments, such as TDTR. We provide one such approach in this paper.

In this work, we performed time-domain nonadiabatic (NA) molecular dynamics (MD) simulations to study the electron−phonon coupling and relaxation dynamics of thin Au films at different temperatures. The ab initio atomistic methodology mimics the pump−probe optical experiments in the most direct way and emphasizes the nonequilibrium nature of the electronic relaxation dynamics. Previously, the time-domain NAMD approach has been applied successfully to a broad range of nanostructural, semiconducting, and metallic systems.[58−69] Here, we report on the effect of temperature on the crystal and electronic structure, NA electron−phonon coupling, and electron relaxation rate using this approach.

2. THEORY AND SIMULATION METHODS

The simulations are performed using a mixed quantum-classical technique, in which the faster electronic degrees of freedom are treated quantum mechanically, while the slower nuclear motions are described classically. The electronic evolution is obtained using a real-time time-dependent (TD) density functional theory (DFT) in the Kohn−Sham (KS) representation.[70] The nuclear evolutions are modeled by classical MD, and the electron−nuclear interactions are obtained using NAMD. The electron relaxation dynamics are modeled with the fewest switching surface hopping (FSSH).[71,72] The original implementation of FSSH within TDDFT in the KS formulation,[73,74] and its adaptation[75−78] to nanoscale and solid-state systems are described in our previous works.

2.1. Time-Dependent Density Functional Theory. The electron density of a system, $\rho(\mathbf{r},t)$, is expressed in the KS representation of DFT as a sum of the densities of single-electron KS orbitals, $\psi_n(\mathbf{r}, t)$, occupied by N_e electrons[79]

$$\rho(\mathbf{r}, t) = \sum_{n=1}^{N_e} |\Psi_n(\mathbf{r}, t)|^2 \tag{1}$$

Applying the time-dependent variational principle to the expectation value of the KS density functional leads to the system of coupled equations of motion for the single-particle KS orbitals[79]

$$i\hbar \frac{\partial}{\partial t}_n (\mathbf{r}, t) = H(\mathbf{r}, \mathbf{R}, t)\Psi_n(\mathbf{r}, t) \tag{2}$$

Here, the Hamiltonian, $H(\mathbf{r},\mathbf{R},t)$, is a functional of the total electron density. The Hamiltonian is time dependent due to the external potential created by the moving atoms and the electric field of a laser. The time-dependent KS orbitals, $\psi_n(\mathbf{r},\mathbf{R},t)$, are expanded in the basis of adiabatic KS orbitals, $\Phi_k(\mathbf{r};\mathbf{R},t)$, which are calculated as eigenstates of the KS Hamiltonian for the current atomic positions, $\mathbf{R}$, obtained from the MD

$$\Psi_n(\mathbf{r}, t) = \sum_k C_k^n(t)_k[\mathbf{r}; \mathbf{R}, (t)] \tag{3}$$

A combination of eq 2 and eq 3 gives equations-of-motion for the expansion coefficients

$$i\hbar \frac{\partial}{\partial t} c_j^n(t) = \sum_k C_k^n(t)(\varepsilon_k \delta_{jk} + d_{jk}) \tag{4}$$

Here, ε_k is the energy of the adiabatic state k and d_{jk} is the electron−phonon NA coupling (NAC) between adiabatic states k and j. The coupling arises from the dependence of

DOI: 10.1021/acs.jpcc.7b05211
J. Phys. Chem. C 2017, 121, 17488−17497

the electronic subsystem on the atomic motion **R**. It is calculated numerically as the overlap between wave functions k and j at sequential time steps

$$d_{jk} = -i\hbar\langle\Phi_j|\nabla_{\mathbf{R}}|\Phi_k\rangle \times \frac{\mathrm{d}\mathbf{R}}{\mathrm{d}t} = -i\hbar\left\langle \Phi_j\left|\frac{\partial}{\partial t}\right|\Phi_k\right\rangle \quad (5)$$

Note that the electron−phonon NAC does not invoke the harmonic phonon approximation.

2.2. Nonadiabatic Dynamics by Surface Hopping. Surface hopping (SH) is a stochastic algorithm for switching electronic states in a mixed quantum-classical simulation. It uses solutions to the time-dependent Schrödinger equation, eq 2, to obtain a master equation with time-dependent transition rates. Motived by failures of the mean-field approximation, known in quantum-classical dynamics as the Ehrenfest approach, SH introduces correlations between the electronic and nuclear evolutions.[80] Most importantly for the current electron−phonon relaxation study, SH gives detailed balance between transitions up and down in energy, properly reproducing Boltzmann statistics in the quantum-classical equilibrium.[72] FSSH is the most popular SH technique since it is applicable to a broad range of systems and processes.[81−86]

FSSH provides a probability for hopping between quantum states based on the evolution of the expansion coefficients, eq 4. The probability of a transition from state j to another state k within the time interval $\mathrm{d}t$ is given in FSSH by[71]

$$\mathrm{d}\mathbf{P}_{jk} = \frac{-2\mathrm{Re}(A_{jk}^* d_{jk}\dot{\mathbf{R}})}{A_{jj}}\mathrm{d}t; \qquad A_{jk} = c_j c_k^* \quad (6)$$

If the calculated $\mathrm{d}\mathbf{P}_{jk}$ is negative, the hopping probability is set to zero: a hop from state j to state k can take place only when the electronic occupation of state j decreases, and the occupation of state k increases. To conserve the total electron−nuclear energy after a hop, the original FSSH technique[71] rescales the nuclear velocities along the direction of the NAC. If a NA transition to a higher energy electronic state is predicted by eq 6, but the kinetic energy available in the nuclear coordinates along the direction of the NAC is insufficient to accommodate the increase in the electronic energy, then the hop is rejected. The velocity rescaling and hop rejection give rise to the detailed balance between transitions upward and downward in energy.[72] The assumption that the energy exchanged between the electronic and nuclear degrees of freedom during the hop is redistributed rapidly and provides the Boltzmann distribution of energy among nuclear modes. Then, the velocity rescaling and hop rejection can be replaced by multiplying the probability, eq 6, for transitions upward in energy by the Boltzmann factor. This simplification gives the classical path approximation to the original FSSH technique.[75,87] It generates great computational savings, allowing one to determine the time-dependent potential that drives multiple FSSH realizations of the dynamics of the electronic subsystem using a single MD trajectory.

In cases involving slow quantum transitions between states significantly separated in energy, FSSH requires decoherence corrections.[76] The current simulations involve rapid transitions within a dense manifold of states (band), and therefore, decoherence corrections are not applied.

2.3. Simulation Details. We employ the plane-wave DFT approach, as implemented in the Vienna Ab initio Simulation Package (VASP), to perform geometry optimization, electronic structure, and adiabatic MD calculations.[88] The nonlocal exchange and correlation contributions to the electronic energy were treated with the Perdew−Burke−Ernzerhof (PBE) functional.[89] The projector-augmented wave (PAW) approach was used to describe the interaction of the ionic cores with the valence electrons.[90] The basis set energy cutoff was set to 400 eV. To simulate Au thin films, we started with the bulk Au structure and constructed a Au(111) surface with seven layers of Au atoms, as depicted in Figure 1. A vacuum layer of 20 Å was added to avoid the interaction between periodic slabs. The Monkhorst−Pack mesh of 5 × 5 × 1 was used for the structural optimization and MD, and 7 × 7 × 1 was used in the DOS calculations.

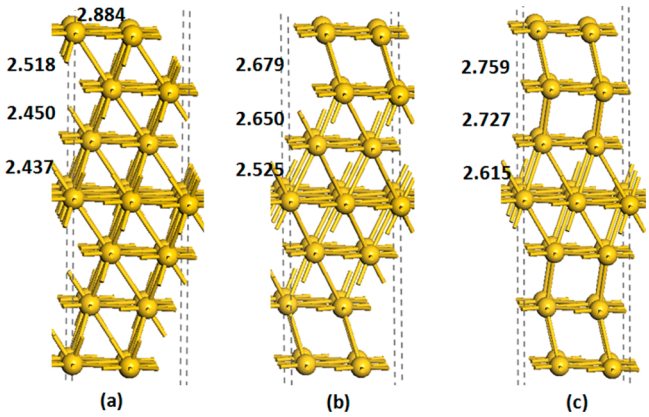

Figure 1. Side view of the simulation cell showing geometry of the Au (111) system (a) optimized at 0 K, and during the molecular dynamics runs at (b) 100 K and (c) 300 K.

After relaxing the geometry at 0 K (Figure 1a), repeated velocity rescaling was used to bring the temperature of the system to 100 or 300 K, corresponding to the temperatures in the experiment.[21] Following a 3 ps thermalization dynamics, 7 ps adiabatic MD simulations were performed in the micro-canonical ensemble with a 1 fs atomic time-step. The adiabatic state energies and NAC were calculated for each step of the MD run. The NAMD calculation was carried out using the quantum-classical FSSH technique implemented[73] within the time-dependent KS scheme[91] with the PYXAID code.[75,76] One-thousand geometries were selected randomly from the adiabatic MD trajectory and were used as initial conditions for NAMD. One-hundred stochastic realizations of the FSSH algorithm were sampled for each initial condition.

3. RESULTS AND DISCUSSION

3.1. Geometric and Electronic Structure. Figure 1 shows a side view of the Au system relaxed at 0 K (Figure 1a) and two snapshots taken from the MD runs at 100 and 300 K (Figure 1, panels b and c, respectively). A comparison of the three panels indicates that thermal fluctuations have a notable impact on the system geometry. The system expands as the temperature grows, and the distances between the Au layers increase. In the geometry optimized at 0 K, the distances between the layers are 2.518, 2.450, and 2.437 Å from the top to the middle of the slab, respectively. At 100 K, the corresponding average distances lengthen to 2.679, 2.650, and 2.525 Å. And at 300 K, the average distances lengthen further to 2.759, 2.727, and 2.615 Å, respectively. The intralayer Au−Au bond length fluctuates around the equilibrium value of 2.884 Å independent of temperature, since the simulation cell size is fixed and the

DOI: 10.1021/acs.jpcc.7b05211
J. Phys. Chem. C 2017, 121, 17488−17497

system is not allowed to expand in the periodic direction. This is a good approximation simplifying the calculations because the fractional expansion coefficient of gold is small, on the order of 10^{-5} per degree Kelvin. A 200 K temperature increase should lead to a 2% cell expansion and a bond length increase by 0.05 Å, which is less than the magnitude of thermally induced bond length fluctuations.

Figure 2 gives the total DOS (TDOS) and projected DOS (PDOS) of the optimized structure. As shown in Figure 2a,

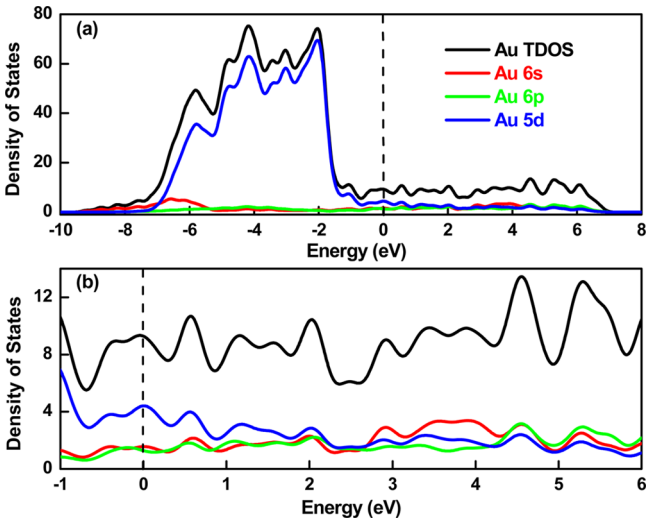

Figure 2. Total and projected densities of states of the Au(111) surface over (a) −10 to 8 eV and (b) −1 to 6 eV energy ranges. The Fermi level is set to zero and is shown by the dashed line.

there is no band gap due to the metallic character of Au. The Fermi level is set to zero. In the energy range between −7 and 0 eV, the contribution of the Au 5*d* states is more significant as compared to the contributions of the Au 6s and 6p states. The situation changes at the Fermi energy, at which the contributions of the Au 6s and 6p states becomes comparable to the Au 5d states contribution. Note that to obtain PDOS, a projection on spherical harmonics is done. In this procedure, part of the information is lost. As a result, the sum of the parts is lower than the whole DOS.

We focus on the pump−probe experiments performed with the excitation energy of 3.1 eV.[21,48] Therefore, we consider electrons up to 3.1 eV above the Fermi level and divide the energy range into the 0−1 eV, 1−2 eV, 2−3 eV increments to analyze the electron−phonon interaction. As shown in Figure 2b, the TDOS magnitude increases in the following series of energy ranges 1−2 eV < 2−3 eV < 0−1 eV. Generally, higher DOS favors larger NAC and results in faster electron−phonon energy relaxation.

Figure 3 presents charge densities of electronic states involved in the electron−phonon relaxation processes considered here. Charge densities at 0, 100, and 300 K are presented. Fluctuations of the energies of these states along the MD trajectory are related to the strength of electron−phonon coupling. The coupling strength is also related to the overlap between wave functions of different states, quantitatively described by eq 5. The density of the highest occupied molecular orbital (HOMO) at the Fermi energy is localized in the middle of the slab at 0 K. As the temperature increases, the density spreads somewhat to the outer regions of the slab. For the state 1 eV above the Fermi level, the density patterns look

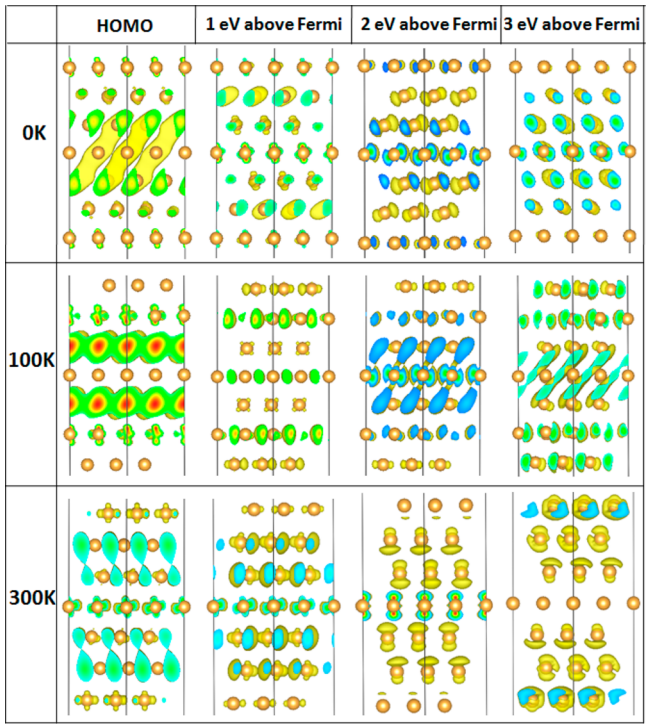

Figure 3. Charge densities of several electronic states: HOMO, and orbitals located 1, 2, and 3 eV above the Fermi level for Au at 0, 100, and 300 K. The iso-surface value is set to 0.001 e/A^3 in all cases.

similar for 0 and 100 K: the density is localized preferentially on the subsurface layers. In comparison, the electronic density expands to all bulk layers at 300 K. As shown in Figure 3, the state located 2 eV above the Fermi energy level contains densities on all inner layers, independent of temperature. As for the state at 3.1 eV above the Fermi level, the charge density spreads from the middle to the side of the model with the increase of temperature. Generally, our results show that temperature has a relatively small effect on the electron wave functions, with somewhat more scatter seen at higher temperatures.

3.2. Nonadiabatic Electron−Phonon Coupling. Electron−phonon relaxation appears in trajectory SH as a sequence of NA transitions between electronic energy levels. Each elementary transition depends on the strength of the NAC. The generated MD trajectories are utilized to compute electron−phonon NAC for all pairs of orbitals spanning 3.1 eV energy above the Fermi level.

Table 1 reports the absolute NAC values, |NAC|, denoted by N^{abs}, and root-mean-square of NAC, denoted by N^{rms}. The NAC values are averaged either over all electron states involved in the relaxation or over only the neighboring states. Different excitation energies are considered in the Au systems at 100 and 300 K. On the basis of eq 5, the NAC depends on the overlap of the electronic wave functions and the nuclear velocity. The nuclear velocity is determined by the frequency and amplitude of vibrations and is temperature-dependent. Since phonon kinetic energy is proportional to temperature, the higher is the vibration frequency, the larger is the velocity at a given temperature.

The data in Table 1 show that the electron−phonon NAC increases as temperature grows from 100 to 300 K. The coupling between nearest states is 2−5 times larger than the coupling averaged over all pairs of states, which means that the

DOI: 10.1021/acs.jpcc.7b05211
J. Phys. Chem. C 2017, 121, 17488−17497

Table 1. Absolute Nonadiabatic Coupling (|NACl|) Averaged over Nearest States ($N^{abs}_{i,i+1}$) and over All States (N^{abs}_{total}), Root-Mean-Square NAC Averaged over Nearest States ($N^{rms}_{i,i+1}$) and over All States (N^{rms}_{total}), Pure-Dephasing Time Averaged over Nearest States ($\tau_{i,i+1}$) and over all states (τ_{total}), and Relaxation Time at 100 and 300 K

	100 K					300 K				
	0−1 eV	0−2 eV	0−3 eV	1−2 eV	2−3 eV	0−1 eV	0−2 eV	0−3 eV	1−2 eV	2−3 eV
$N^{abs}_{i,i+1}$ (meV)	5.60	4.84	4.57	2.08	4.48	7.15	6.64	6.19	4.99	5.90
N^{abs}_{total} (meV)	1.88	1.44	0.93	1.50	1.35	2.60	1.84	1.26	2.30	1.95
$N^{rms}_{i,i+1}$ (meV)	37.60	33.84	32.82	20.39	32.83	46.91	44.59	42.37	37.02	40.97
N^{rms}_{total} (meV)	10.90	8.36	5.36	13.11	10.27	15.37	11.00	7.43	19.71	15.15
$\tau_{i,i+1}$ (fs)	12.0	10.3	9.0	3.6	7.6	10.2	9.0	8.3	5.7	6.8
τ_{total} (fs)	7.6	6.1	5.1	3.4	5.4	7.5	5.9	4.7	4.3	5.0
relaxation (ps)			2.04					1.83		

main contribution to the carrier relaxation should come from transitions between neighboring states involving small energy increments. The N^{abs} values are nearly an order of magnitude smaller than the N^{rms} values, indicating that NAC fluctuates significantly. Considering Fermi's golden rule, the transitions rate depends on NAC squared, which is directly related to N^{rms}. Therefore, the N^{rms} values are better indicators of the strength of the electron−phonon coupling than N^{abs}. The fluctuation in the NAC values is a consequence of the adiabatic quantum-classical representation for the electron−phonon relaxation dynamics, which is most natural in ab initio calculations. In the adiabatic picture, the electron−phonon coupling is strongest when the energy of the active modes is concentrated in the kinetic energy component, and the velocity entering NAC, eq 5, is large.

NAC decreases slightly with increasing energy at both temperatures. The NAC is small in the 1−2 eV energy range, Table 1, in correlation with the drop in the corresponding DOS, Figure 2. A higher state density not only provides more relaxation channels but also favors larger NAC. This is because the overlap-type term encountered in the NAC, eq 5, is generally larger for states that are close in energy and have similar wave functions.

Figure 4 presents the evolution of the energy of the photoexcited electron, which is excited at slightly above 3 eV and relaxes to the Fermi energy by coupling to phonons. The data show that the early stage of the dynamics is Gaussian,

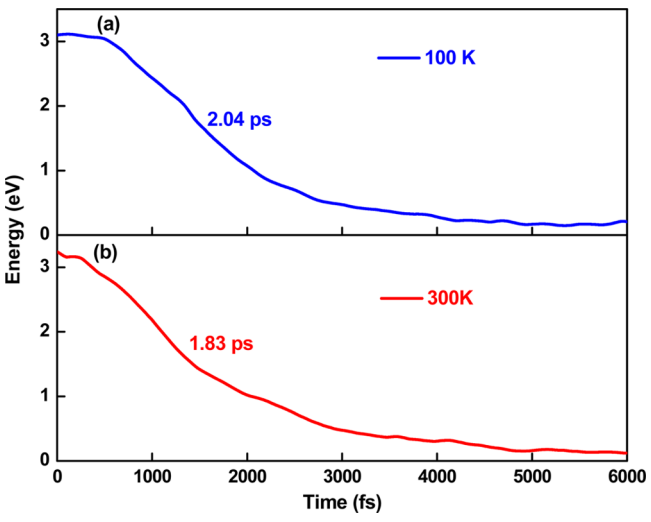

Figure 4. Average electron energy decay in the Au system at (a) 100 K and (b) 300 K.

representing the regime in which the initial state couples to a few other states. The initial Gaussian component is closely related to the cosinusoidal Rabi oscillation that is observed in two-level systems. The fact that the time-derivative of the dynamics data is zero at $t = 0$ is essential for the quantum Zeno effect,[63] stating that the dynamics stop if one attempts to measure the state of the system very frequently. The Gaussian component is larger at the lower temperature, because the NAC is smaller, and the dynamics require more time to involve a large number of states. Once the dynamics involve many electronic states, the evolution becomes exponential. Because the exponential component of the electron energy loss is dominant in magnitude, we fit the data to the exponential function, $E(T) = E_0 \exp(-t/\tau)$, for simplicity.

The current study focuses on dynamics of photoexcited electrons. In a future work, we plan to evaluate the hole dynamics, which is likely to be different, in particular, since the hole DOS rises rapidly at energies below −1.8 eV, Figure 2a.

3.3. Converting Nonadiabatic Coupling to Thermodynamic Units. Microscopic calculations provide electron−phonon coupling values in units of energy, presently meV. Thermodynamic models[47,54−56,92] describe how much energy is exchanged between electrons and phonons per unit time, per unit volume and per degree Kelvin, resulting in the units of $Wm^{-3}\,K^{-1}$. Even though the NAC computed here and G_{eff} used in the thermodynamics models are not equivalent, it is instructive to convert the NAC values to the units of G_{eff}. In order to convert the units, we need to know the rate of energy losses and the system volume. The latter is the volume occupied by the Au film in the simulation cell, depicted in Figure 1 (which is equal to 983 $Å^3$). The rate of energy loss is estimated by performing the FSSH simulations of the phonon-induced relaxation of the electron energy starting at 3.1 eV above the Fermi level, as in the experiments.[21] Exponential fitting of the simulation data, Figure 4, produce a 2.04 ps time scale at 100 K versus 1.83 ps at 300 K, Table 1, in agreement with the previous simulations on metal clusters.[93−95] The conversion from NAC to G_{eff} is performed as exemplified with the first entries of Tables 1 and 2. The 5.60 meV NAC value from Table 1 is multiplied by the electron−phonon energy exchange rate 1 eV/2.04 ps and divided by the volume 983 $Å^3$. Converting to the SI units gives 4.468×10^{17} Wm^{-3} K in Table 2.

The G_{eff} values obtained here agree well with the earlier ab initio calculations of Zhigilei and co-workers[54] but are an order of magnitude higher than the values deduced from the recent experiments.[21] It should be emphasized that the NAC defined in eq 5 and the electron−phonon scattering matrix elements used the thermodynamic models,[47,54−56,92] for instance $M_{kk'}$ in

DOI: 10.1021/acs.jpcc.7b05211
J. Phys. Chem. C 2017, 121, 17488−17497

Table 2. Absolute Nonadiabatic Coupling, Table 1, Expressed in Units of Effective Electron-Phonon Coupling, G_{eff}

	100 K					300 K				
(10^{17}W/m^{3}K)	0−1 eV	0−2 eV	0−3 eV	1−2 eV	2−3 eV	0−1 eV	0−2 eV	0−3 eV	1−2 eV	2−3 eV
$G_{eff}^{abs}{}_{i,i+1}$	4.468	3.862	3.646	1.660	3.574	6.359	5.906	5.506	4.438	5.248
$G_{eff}^{abs}{}_{total}$	1.500	1.149	0.742	1.197	1.077	2.313	1.637	1.121	2.046	1.734

eq 6 of ref 54 represent the same physical process, but are not equivalent. The NAC matrix elements appear in as a result of the adiabatic, Born−Oppenheimer representation arising naturally in the ab initio electronic structure theory and used subsequently in the NAMD simulations. The calculation of the NAC matrix elements does not invoke the harmonic approximation for the phonons, which is particularly important for soft matter, liquids, and molecular systems. The NAC is time-dependent, since it is computed on-the-fly along an MD trajectory. It fluctuates significantly due to fluctuations in the nuclear velocities, $\frac{d\mathbf{R}}{dt}$, eq 5, and that is why the absolute average values and the root-mean-square values differ significantly, Table 1. In contrast, the electron−phonon scattering matrix elements invoke the harmonic approximation for the phonons, which assumes that the system is in its optimal, lowest-energy geometry, and are time-independent. Further, the G_{eff} values obtained in ref 54 and related models[2,47,55,56,92] make the quasi-equilibrium assumptions for the distribution of the electron and phonon energies, while NAMD simulations make no such assumption and produce truly nonequilibrium dynamics. At the same time, NAMD simulations are significantly more computationally expensive, in particular, since they require thousands of electronic structure and electron−phonon coupling calculations for each time-step along the NAMD trajectories.

3.4. Elastic Electron−Phonon Scattering. Electron−phonon interactions are responsible for both elastic and inelastic electron−phonon scattering. Inelastic scattering results in energy exchange between the electronic and vibrational degrees of freedom. The strength of the inelastic electron−phonon interaction is reflected in the magnitudes of the NAC and G_{eff} matrix elements, Tables 1 and 2. Elastic electron−phonon scattering does not involve energy exchange. Rather, it induces loss of coherence within the electronic subsystem by randomizing the phase of the electronic wave function.

Elastic electron−phonon scattering is known in optical measurements as pure-dephasing.[96−100] The inverse of the pure-dephasing time gives the line width of optical transitions at the single particle (homogeneous) level of measurement. We estimate the time-scale of the elastic electron−phonon scattering using the optical response theory[96−100] by computing the pure-dephasing time for all pairs of electronic states under consideration. The pure-dephasing times averaged over nearest neighbor and all pairs of states are shown in Table 1. The pure-dephasing time is shorter at the higher temperature, indicating that the strength of the elastic electron−phonon scattering increases with temperature, similarly to the strength of the inelastic scattering. The pure-dephasing times averaged only over pairs of nearest electronic states are longer than the times averaged over all pairs of states, showing that phonon-induced loss of quantum coherence within the electronic subsystem becomes faster as the energy difference between the initial and final electronic states increases.

3.5. Active Phonon Modes. To obtain further insights into the electron−phonon scattering, we identified the phonon modes that couple to the electronic subsystem. For this purpose, we calculated Fourier transforms (FTs) of the autocorrelation functions of the energy gaps between representative pairs of electronic states. The result is known as the spectral density or the influence spectrum.[101,102] The FTs characterize the frequencies of the phonon modes that induce electron−phonon scattering and accommodate the electronic energy lost during the transitions. The magnitude of each peak in the FT spectrum reflects the strength of the electron−phonon coupling for that phonon frequency.

Figure 5 shows the spectral densities computed for different temperatures and energy gaps between initial and final

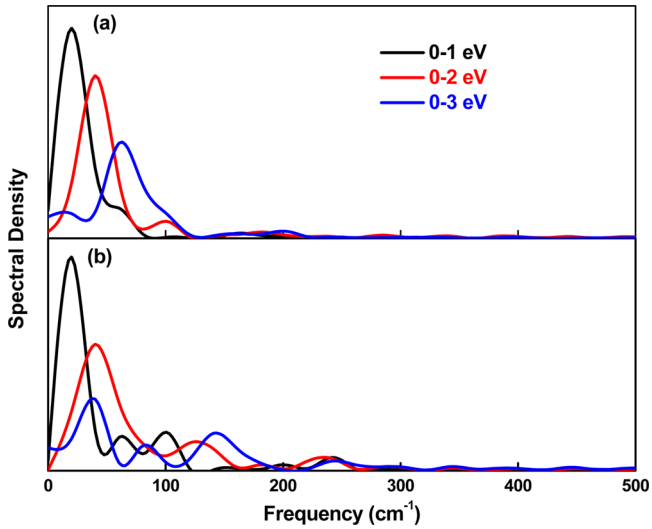

Figure 5. Fourier transforms of the energy gaps from the Fermi level to electronic levels at 1, 2, and 3 eV above it, at (a) 100 K and (b) 300 K.

electronic states. Considering the energy gaps, we observe that the FT magnitudes vary in the sequence 0−1 eV > 0−2 eV> 0−3 eV at both 100 and 300 K. The variation agrees well with the corresponding trend in the NAC values shown in Table 1. An increase in temperature broadens the coupling spectra, creating tails that extend into the higher frequency range (cf. Figure 5, panels a and b). More phonon modes are able to couple to the electronic subsystem, enhancing the overall electron−phonon coupling. Participation of higher frequency phonons at the elevated temperature can be rationalized by thermal excitation of these modes and by anharmonic effects that relax the electron−phonon coupling selection rules.

The notable peaks below 100 cm^{-1} in the phonon spectra shown in Figure 5 can be assigned to acoustic phonon modes that have been observed in gold clusters[103] and films.[104] The higher frequencies observed in the 300 K spectrum (Figure 5b) can be attributed to longitudinal and transverse optical phonons with the experimental[105] frequencies extending to 4.70 THz (or 157 cm^{-1}). The tails beyond 200 cm^{-1} are associated with overtones of these modes.

DOI: 10.1021/acs.jpcc.7b05211
J. Phys. Chem. C 2017, 121, 17488−17497

4. CONCLUSIONS

We have performed a time-domain atomistic investigation of electron−phonon relaxation dynamics in thin gold films at different temperatures. The simulations were carried out using ab initio nonadiabatic molecular dynamics that mimics most directly the nonequilibrium nature of the relaxation processes, including anharmonicity of vibrational motions, realistic density of electronic states, and dependence on excitation energy and temperature. We computed and analyzed the nonadiabatic electron−phonon coupling matrix elements responsible for inelastic electron−phonon scattering and the pure-dephasing times representing elastic scattering. The nonadiabatic couplings expressed in energy units were converted to the units of energy per unit time, unit volume, and degree Kelvin, for comparison with the effective electron−phonon coupling used in engineering calculations and representing volumetric rate of energy transfer between a pair of states. The simulation results were also compared to the corresponding time-resolved experimental measurements.

It was found that the electron−phonon coupling grows with increasing temperature, in agreement with the experiment.[21] The finding applies to both inelastic and elastic electron−phonon scattering processes and can be rationalized by participation of a broader spectrum of phonon modes at the elevated temperature. Higher temperatures are capable of activating higher frequency phonons and to increase anharmonicity that relaxes electron−phonon coupling selection rules. The gold films expand at higher temperatures, pushing the system away from the equilibrium geometry. The electron−phonon coupling between electronic states that are close in energy is a factor of 2−5 stronger than the coupling between states that are distant in energy, indicating that electron-vibrational energy relaxation proceeds by rapid transitions in small energy increments. The strongest coupling is induced by low-frequency acoustic phonons. In contrast to the inelastic electron−phonon scattering that occur more rapidly between nearest states, the elastic scattering occurs faster between states that are more distant in energy. The results presented in this paper emphasize the nonequilibrium nature of the relaxation dynamics and facilitate the understanding of the fundamental mechanisms of electron−phonon energy exchange in thin metal films, guiding future experiments.

AUTHOR INFORMATION

Corresponding Author

*E-mail: prezhdo@usc.edu.

ORCID

Ashutosh Giri: 0000-0002-8899-4964

Oleg V. Prezhdo: 0000-0002-5140-7500

Notes

The authors declare no competing financial interest.

ACKNOWLEDGMENTS

X.Z. and H.D. acknowledge support of the National Natural Science Foundation of China, Grants 21473183 and 21303079, and China Scholarship Council. L.L., A.G., P.E.H., and O.V.P. acknowledge funding from the U.S. Department of Defense, Multidisciplinary University Research Initiative, Grant W911NF-16-1-0406.

REFERENCES

(1) Morrison, A. F.; Herbert, J. M. Evidence for Singlet Fission Driven by Vibronic Coherence in Crystalline Tetracene. *J. Phys. Chem. Lett.* **2017**, *8*, 1442−1448.

(2) Allen, P. B. Theory of Thermal Relaxation of Electrons in Metals. *Phys. Rev. Lett.* **1987**, *59*, 1460−1463.

(3) Yang, H.; Gajdos, F.; Blumberger, J. Intermolecular Charge Transfer Parameters, Electron-Phonon Couplings, and the Validity of Polaron Hopping Models in Organic Semiconducting Crystals: Rubrene, Pentacene, and C-60. *J. Phys. Chem. C* **2017**, *121*, 7689−7696.

(4) Karakus, M.; Jensen, S. A.; D'Angelo, F.; Turchinovich, D.; Bonn, M.; Canovas, E. Phonon-Electron Scattering Limits Free Charge Mobility in Methylammonium Lead Iodide Perovskites. *J. Phys. Chem. Lett.* **2015**, *6*, 4991−4996.

(5) Sinova, J. Spin Seebeck Effect: Thinks Globally but Acts Locally. *Nat. Mater.* **2010**, *9*, 880−881.

(6) Bauer, G. E. W.; Saitoh, E.; van Wees, B. J. Spin Caloritronics. *Nat. Mater.* **2012**, *11*, 391−399.

(7) Long, R.; Fang, W. H.; Akimov, A. V. Nonradiative Electron-Hole Recombination Rate Is Greatly Reduced by Defects in Monolayer Black Phosphorus: Ab Initio Time Domain Study. *J. Phys. Chem. Lett.* **2016**, *7*, 653−659.

(8) Mondal, T.; Tripathi, A.; Zhang, J. Y.; Shripathi, T.; Shinohara, H.; Tiwari, A. Thermal Conductivity of M@C-82 M = Dy, Gd Thin Films. *J. Phys. Chem. C* **2017**, *121*, 3642−3647.

(9) Ivanov, D. S.; Zhigilei, L. V. Combined Atomistic-Continuum Modeling of Short-Pulse Laser Melting and Disintegration of Metal Films. *Phys. Rev. B: Condens. Matter Mater. Phys.* **2003**, *68*, 064114.

(10) Zarick, H. F.; Boulesbaa, A.; Talbert, E. M.; Puretzky, A.; Geohegan, D.; Bardhan, R. Ultrafast Excited-State Dynamics in Shape- and Composition-Controlled Gold-Silver Bimetallic Nanostructures. *J. Phys. Chem. C* **2017**, *121*, 4540−4547.

(11) Chan, W.-L.; Averback, R. S.; Cahill, D. G.; Lagoutchev, A. Dynamics of Femtosecond Laser-Induced Melting of Silver. *Phys. Rev. B: Condens. Matter Mater. Phys.* **2008**, *78*, 214107.

(12) Chan, W.-L.; Averback, R. S.; Cahill, D. G.; Ashkenazy, Y. Solidification Velocities in Deeply Undercooled Silver. *Phys. Rev. Lett.* **2009**, *102*, 095701.

(13) Hartland, G. V. Optical Studies of Dynamics in Noble Metal Nanostructures. *Chem. Rev.* **2011**, *111*, 3858−3887.

(14) Ochoa, M. A.; Selzer, Y.; Peskin, U.; Galperin, M. Pump-Probe Noise Spectroscopy of Molecular Junctions. *J. Phys. Chem. Lett.* **2015**, *6*, 470−476.

(15) Elsayed-Ali, H. E.; Norris, T. B.; Pessot, M. A.; Mourou, G. A. Time-Resolved Observation of Electron-Phonon Relaxation in Copper. *Phys. Rev. Lett.* **1987**, *58*, 1212−1215.

(16) Elsayed-Ali, H. E.; Juhasz, T.; Smith, G. O.; Bron, W. E. Femtosecond Thermoreflectivity and Thermotransmissivity of Polycrystalline and Single-Crystalline Gold Films. *Phys. Rev. B: Condens. Matter Mater. Phys.* **1991**, *43*, 4488−4491.

(17) Schnedermann, C.; Lim, J. M.; Wende, T.; Duarte, A. S.; Ni, L. M.; Gu, Q. F.; Sadhanala, A.; Rao, A.; Kukura, P. Sub-10 Fs Time-Resolved Vibronic Optical Microscopy. *J. Phys. Chem. Lett.* **2016**, *7*, 4854−4859.

(18) Gdor, I.; Ghosh, T.; Lioubashevski, O.; Ruhman, S. Non-resonant Raman Effects on Femtosecond Pump-Probe with Chirped White Light: Challenges and Opportunities. *J. Phys. Chem. Lett.* **2017**, *8*, 1920−1924.

(19) Del Fatti, N.; Voisin, C.; Achermann, M.; Tzortzakis, S.; Christofilos, D.; Vallée, F. Nonequilibrium Electron Dynamics in Noble Metals. *Phys. Rev. B: Condens. Matter Mater. Phys.* **2000**, *61*, 16956−16966.

(20) Courtney, T. L.; Fox, Z. W.; Estergreen, L.; Khalil, M. Measuring Coherently Coupled Intramolecular Vibrational and Charge-Transfer Dynamics with Two-Dimensional Vibrational Electronic Spectroscopy. *J. Phys. Chem. Lett.* **2015**, *6*, 1286−1292.

(21) Giri, A.; Gaskins, J. T.; Foley, B. M.; Cheaito, R.; Hopkins, P. E. Experimental Evidence of Excited Electron Number Density and

DOI: 10.1021/acs.jpcc.7b05211
J. Phys. Chem. C 2017, 121, 17488−17497

Temperature Effects on Electron-Phonon Coupling in Gold Films. *J. Appl. Phys.* **2015**, *117*, 044305.
(22) Groeneveld, R. H. M.; Sprik, R.; Lagendijk, A. Ultrafast Relaxation of Electrons Probed by Surface Plasmons at a Thin Silver Film. *Phys. Rev. Lett.* **1990**, *64*, 784−787.
(23) Groeneveld, R. H. M.; Sprik, R.; Lagendijk, A. Effect of a Nonthermal Electron Distribution on the Electron-Phonon Energy Relaxation Process in Noble Metals. *Phys. Rev. B: Condens. Matter Mater. Phys.* **1992**, *45*, 5079−5082.
(24) Groeneveld, R. H. M.; Sprik, R.; Lagendijk, A. Femtosecond Spectroscopy of Electron-Electron and Electron-Phonon Energy Relaxation in Ag and Au. *Phys. Rev. B: Condens. Matter Mater. Phys.* **1995**, *51*, 11433−11445.
(25) Bonn, M.; Denzler, D. N.; Funk, S.; Wolf, M.; Wellershoff, S.-S.; Hohlfeld, J. Ultrafast Electron Dynamics at Metal Surfaces: Competition between Electron-Phonon Coupling and Hot-Electron Transport. *Phys. Rev. B: Condens. Matter Mater. Phys.* **2000**, *61*, 1101−1105.
(26) Hohlfeld, J.; Muller, J. G.; Wellershoff, S.-S.; Matthias, E. Time-Resolved Thermoreflectivity of Thin Gold Films and Its Dependence on Film Thickness. *Appl. Phys. B: Lasers Opt.* **1997**, *64*, 387−390.
(27) Hohlfeld, J.; Wellershoff, S. S.; Gudde, J.; Conrad, U.; Jahnke, V.; Matthias, E. Electron and Lattice Dynamics Following Optical Excitation of Metals. *Chem. Phys.* **2000**, *251*, 237−258.
(28) Sun, C. K.; Vallee, F.; Acioli, L. H.; Ippen, E. P.; Fujimoto, J. G. Femtosecond Investigation of Electron Thermalization in Gold. *Phys. Rev. B: Condens. Matter Mater. Phys.* **1993**, *48*, 12365−12368.
(29) Sun, C. K.; Vallee, F.; Acioli, L. H.; Ippen, E. P.; Fujimoto, J. G. Femtosecond-Tunable Measurement of Electron Thermalization in Gold. *Phys. Rev. B: Condens. Matter Mater. Phys.* **1994**, *50*, 15337−15348.
(30) Wellershoff, S.-S.; Hohlfeld, J.; Gudde, J.; Matthias, E. The Role of Electron-Phonon Coupling in Femtosecond Laser Damage of Metals. *Appl. Phys. A: Mater. Sci. Process.* **1999**, *69*, S99−S107.
(31) Fann, W. S.; Storz, R.; Tom, H. W. K.; Bokor, J. Direct Measurement of Nonequilibrium Electron-Energy Distributions in Subpicosecond Laser-Heated Gold Films. *Phys. Rev. Lett.* **1992**, *68*, 2834−2837.
(32) Fann, W. S.; Storz, R.; Tom, H. W. K.; Bokor, J. Electron Thermalization in Gold. *Phys. Rev. B: Condens. Matter Mater. Phys.* **1992**, *46*, 13592−13595.
(33) Wang, X. Y.; Riffe, D. M.; Lee, Y.-S.; Downer, M. C. Time-Resolved Electron-Temperature Measurement in a Highly Excited Gold Target Using Femtosecond Thermionic Emission. *Phys. Rev. B: Condens. Matter Mater. Phys.* **1994**, *50*, 8016−1019.
(34) Hopkins, P. E.; Klopf, J. M.; Norris, P. M. Influence of Interband Transitions on Electron-Phonon Coupling Measurements in Ni Films. *Appl. Opt.* **2007**, *46*, 2076−2083.
(35) Hopkins, P. E.; Norris, P. M. Substrate Influence in Electron-Phonon Coupling Measurements in Thin Au Films. *Appl. Surf. Sci.* **2007**, *253*, 6289−6294.
(36) Hopkins, P. E.; Kassebaum, J. L.; Norris, P. M. Effects of Electron Scattering at Metal-Nonmetal Interfaces on Electron-Phonon Equilibration in Gold Films. *J. Appl. Phys.* **2009**, *105*, 023710.
(37) Hopkins, P. E.; Phinney, L. M.; Serrano, J. R. Reexamining Electron-Fermi Relaxation in Gold Films with a Nonlinear Thermoreflectance Model. *J. Heat Transfer* **2011**, *133*, 044505.
(38) Anisimov, S. I.; Kapeliovich, B. L.; Perel'man, T. L. Electron Emission from Metal Surfaces Exposed to Ultrashort Laser Pulses. *Zh. Eksp. Teor. Fiz.* **1974**, *66*, 776−781.
(39) Zhigilei, L. V.; Ivanov, D. S.; Leveugle, E.; Sadigh, B.; Bringa, E. M. Computer Modeling of Laser Melting and Spallation of Metal Targets. *Proc. SPIE* **2004**, *5448*, 505−519.
(40) Eesley, G. L. Observation of Nonequilibrium Electron Heating in Copper. *Phys. Rev. Lett.* **1983**, *51*, 2140−2143.
(41) Kaganov, M. I.; Lifshitz, I. M.; Tanatarov, L. V. Relaxation between Electrons and the Crystalline Lattice. *Sov. Phys. JETP* **1957**, *4*, 173−178.
(42) Eesley, G. L. Generation of Nonequlibrium Electron and Lattice Temperatures in Copper by Picosecond Laser Pulses. *Phys. Rev. B: Condens. Matter Mater. Phys.* **1986**, *33*, 2144−2151.
(43) Schoenlein, R. W.; Lin, W. Z.; Fujimoto, J. G.; Eesley, G. L. Femtosecond Studies of Nonequilibrium Electronic Processes in Metals. *Phys. Rev. Lett.* **1987**, *58*, 1680−1683.
(44) Brorson, S. D.; Fujimoto, J. G.; Ippen, E. P. Femtosecond Electronic Heat-Transport Dynamics in Thin Gold Films. *Phys. Rev. Lett.* **1987**, *59*, 1962−1965.
(45) Brorson, S. D.; Kazeroonian, A.; Moodera, J. S.; Face, D. W.; Cheng, T. K.; Ippen, E. P.; Dresselhaus, M. S.; Dresselhaus, G. Femtosecond Room-Temperature Measurement of the Electron-Phonon Coupling Constant γ in Metallic Superconductors. *Phys. Rev. Lett.* **1990**, *64*, 2172−2175.
(46) Mihailidi, M.; Xing, Q.; Yoo, K. M.; Alfano, R. R. Electron-Phonon Relaxation Dynamics of Niobium Metal as a Function of Temperature. *Phys. Rev. B: Condens. Matter Mater. Phys.* **1994**, *49*, 3207−3212.
(47) Chen, J. K.; Latham, W. P.; Beraun, J. E. The Role of Electron−Phonon Coupling in Ultrafast Laser Heating. *J. Laser Appl.* **2005**, *17*, 63−68.
(48) Giri, A.; Hopkins, P. E. Transient Thermal and Nonthermal Electron and Phonon Relaxation after Short-Pulsed Laser Heating of Metals. *J. Appl. Phys.* **2015**, *118*, 215101.
(49) Hopkins, P. E. Contributions of Inter- and Intraband Excitations to Electron Heat Capacity and Electron-Phonon Coupling in Noble Metals. *J. Heat Transfer* **2010**, *132*, 014504.
(50) Hopkins, P. E. Influence of Inter- and Intraband Transitions to Electron Temperature Decay in Noble Metals after Short-Pulsed Laser Heating. *J. Heat Transfer* **2010**, *132*, 122402.
(51) Longo, S.; Pietanza, L. D.; Tassielli, F. A.; Capitelli, M. Nonequilibrium Electron Energy Distribution in Au under Subpicosecond Laser Irradiation: A Kinetic Study. *Laser Part. Beams* **2002**, *20*, 285−290.
(52) Pietanza, L. D.; Colonna, G.; Longo, S.; Capitelli, M. Electron and Phonon Distribution Relaxation in Metal Films under a Femtosecond Laser Pulse. *Thin Solid Films* **2004**, *453*−*454*, 506−512.
(53) Rethfeld, B.; Kaiser, A.; Vicanek, M.; Simon, G. Ultrafast Dynamics of Nonequilibrium Electrons in Metals under Femtosecond Laser Irradiation. *Phys. Rev. B: Condens. Matter Mater. Phys.* **2002**, *65*, 214303.
(54) Lin, Z.; Zhigilei, L. V.; Celli, V. Electron-Phonon Coupling and Electron Heat Capacity of Metals under Conditions of Strong Electron-Phonon Nonequilibrium. *Phys. Rev. B: Condens. Matter Mater. Phys.* **2008**, *77*, 075133.
(55) Mueller, B. Y.; Rethfeld, B. Relaxation Dynamics in Laser-Excited Metals under Nonequilibrium Conditions. *Phys. Rev. B: Condens. Matter Mater. Phys.* **2013**, *87*, 035139.
(56) Mueller, B. Y.; Rethfeld, B. Nonequilibrium Electron-Phonon Coupling after Ultrashort Laser Excitation of Gold. *Appl. Surf. Sci.* **2014**, *302*, 24−28.
(57) Hopkins, P. E.; Duda, J. C.; Kaehr, B.; Zhou, X. W.; Yang, C.-Y. P.; Jones, R. E. Ultrafast and Steady-State Laser Heating Effects on Electron Relaxation and Phonon Coupling Mechanisms in Thin Gold Films. *Appl. Phys. Lett.* **2013**, *103*, 211910.
(58) Jankowska, J.; Prezhdo, O. V. Ferroelectric Alignment of Organic Cations Inhibits Nonradiative Electron−Hole Recombination in Hybrid Perovskites: Ab Initio Nonadiabatic Molecular Dynamics. *J. Phys. Chem. Lett.* **2017**, *8*, 812−818.
(59) Duncan, W. R.; Prezhdo, O. V. Nonadiabatic Molecular Dynamics Study of Electron Transfer from Alizarin to the Hydrated Ti4+ Ion. *J. Phys. Chem. B* **2005**, *109*, 17998−18002.
(60) Kilina, S. V.; Kilin, D. S.; Prezhdo, V. V.; Prezhdo, O. V. Theoretical Study of Electron-Phonon Relaxation in Pbse and Cdse Quantum Dots: Evidence for Phonon Memory. *J. Phys. Chem. C* **2011**, *115*, 21641−21651.
(61) Chaban, V. V.; Prezhdo, V. V.; Prezhdo, O. V. Covalent Linking Greatly Enhances Photoinduced Electron Transfer in Fullerene-

DOI: 10.1021/acs.jpcc.7b05211
J. Phys. Chem. C 2017, 121, 17488−17497

Quantum Dot Nanocomposites: Time-Domain Ab Initio Study. *J. Phys. Chem. Lett.* **2013**, *4*, 1−6.
(62) Hyeon-Deuk, K.; Prezhdo, O. V. Multiple Exciton Generation and Recombination Dynamics in Small Si and Cdse Quantum Dots: An Ab Initio Time-Domain Study. *ACS Nano* **2012**, *6*, 1239−1250.
(63) Kilina, S. V.; Neukirch, A. J.; Habenicht, B. F.; Kilin, D. S.; Prezhdo, O. V. Quantum Zeno Effect Rationalizes the Phonon Bottleneck in Semiconductor Quantum Dots. *Phys. Rev. Lett.* **2013**, *110*, 180404.
(64) Akimov, A. V.; Prezhdo, O. V. Nonadiabatic Dynamics of Charge Transfer and Singlet Fission at the Pentacene/C_{60} Interface. *J. Am. Chem. Soc.* **2014**, *136*, 1599−1608.
(65) Akimov, A. V.; Asahi, R.; Jinnouchi, R.; Prezhdo, O. V. What Makes the Photocatalytic Co2 Reduction on N-Doped Ta_2O_5 Efficient: Insights from Nonadiabatic Molecular Dynamics. *J. Am. Chem. Soc.* **2015**, *137*, 11517−11525.
(66) Chaban, V. V.; Pal, S.; Prezhdo, O. V. Laser-Induced Explosion of Nitrated Carbon Nanotubes: Nonadiabatic and Reactive Molecular Dynamics Simulations. *J. Am. Chem. Soc.* **2016**, *138*, 15927−15934.
(67) Kilin, D. S.; Tsemekhman, K.; Prezhdo, O. V.; Zenkevich, E. I.; von Borczyskowski, C. Ab Initio Study of Exciton Transfer Dynamics from a Core-Shell Semiconductor Quantum Dot to a Porphyrin-Sensitizer. *J. Photochem. Photobiol., A* **2007**, *190*, 342−351.
(68) Akimov, A. V.; Muckerman, J. T.; Prezhdo, O. V. Nonadiabatic Dynamics of Positive Charge During Photocatalytic Water Splitting on Gan(10−10) Surface: Charge Localization Governs Splitting Efficiency. *J. Am. Chem. Soc.* **2013**, *135*, 8682−8691.
(69) Guo, Z. Y.; Prezhdo, O. V.; Hou, T. J.; Chen, X.; Lee, S. T.; Li, Y. Y. Fast Energy Relaxation by Trap States Decreases Electron Mobility in Tio2 Nanotubes: Time-Domain Ab Lnitio Analysis. *J. Phys. Chem. Lett.* **2014**, *5*, 1642−1647.
(70) Runge, E.; Gross, E. K. U. Density-Functional Theory for Time-Dependent Systems. *Phys. Rev. Lett.* **1984**, *52*, 997−1000.
(71) Tully, J. C. Molecular Dynamics with Electronic Transitions. *J. Chem. Phys.* **1990**, *93*, 1061−1071.
(72) Parandekar, P. V.; Tully, J. C. Mixed Quantum-Classical Equilibrium. *J. Chem. Phys.* **2005**, *122*, 094102.
(73) Craig, C. F.; Duncan, W. R.; Prezhdo, O. V. Trajectory Surface Hopping in the Time-Dependent Kohn-Sham Approach for Electron-Nuclear Dynamics. *Phys. Rev. Lett.* **2005**, *95*, 163001.
(74) Fischer, S. A.; Habenicht, B. F.; Madrid, A. B.; Duncan, W. R.; Prezhdo, O. V. Regarding the Validity of the Time-Dependent Kohn−Sham Approach for Electron-Nuclear Dynamics Via Trajectory Surface Hopping. *J. Chem. Phys.* **2011**, *134*, 024102.
(75) Akimov, A. V.; Prezhdo, O. V. The Pyxaid Program for Non-Adiabatic Molecular Dynamics in Condensed Matter Systems. *J. Chem. Theory Comput.* **2013**, *9*, 4959−4972.
(76) Akimov, A. V.; Prezhdo, O. V. Advanced Capabilities of the Pyxaid Program: Integration Schemes, Decoherence Effects, Multi-excitonic States, and Field-Matter Interaction. *J. Chem. Theory Comput.* **2014**, *10*, 789−804.
(77) Pal, S.; Trivedi, D. J.; Akimov, A. V.; Aradi, B.; Frauenheim, T.; Prezhdo, O. V. Nonadiabatic Molecular Dynamics for Thousand Atom Systems: A Tight-Binding Approach toward Pyxaid. *J. Chem. Theory Comput.* **2016**, *12*, 1436−1448.
(78) Nebgen, B.; Prezhdo, O. V. Fragment Molecular Orbital Nonadiabatic Molecular Dynamics for Condensed Phase Systems. *J. Phys. Chem. A* **2016**, *120*, 7205−7212.
(79) Marques, M. A. L.; Gross, E. K. U. Time-Dependent Density Functional Theory. *Annu. Rev. Phys. Chem.* **2004**, *55*, 427−455.
(80) Tully, J. C.; Preston, R. K. Trajectory Surface Hopping Approach to Nonadiabatic Molecular Collisions: The Reaction of H^+ with D_2. *J. Chem. Phys.* **1971**, *55*, 562−572.
(81) Duncan, W. R.; Craig, C. F.; Prezhdo, O. V. Time-Domain Ab Initio Study of Charge Relaxation and Recombination in Dye-Sensitized TiO_2. *J. Am. Chem. Soc.* **2007**, *129*, 8528−8543.
(82) Habenicht, B. F.; Prezhdo, O. V. Nonradiative Quenching of Fluorescence in a Semiconducting Carbon Nanotube: A Time-Domain Ab Initio Study. *Phys. Rev. Lett.* **2008**, *100*, 197402.
(83) Fischer, S. A.; Duncan, W. R.; Prezhdo, O. V. Ab Initio Nonadiabatic Molecular Dynamics of Wet-Electrons on the TiO_2 Surface. *J. Am. Chem. Soc.* **2009**, *131*, 15483−15491.
(84) Hyeon-Deuk, K.; Prezhdo, O. V. Time-Domain Ab Initio Study of Auger and Phonon-Assisted Auger Processes in a Semiconductor Quantum Dot. *Nano Lett.* **2011**, *11*, 1845−1850.
(85) Habenicht, B. F.; Prezhdo, O. V. Ab Initio Time-Domain Study of the Triplet State in a Semiconducting Carbon Nanotube: Intersystem Crossing, Phosphorescence Time, and Line Width. *J. Am. Chem. Soc.* **2012**, *134*, 15648−15651.
(86) Long, R.; English, N. J.; Prezhdo, O. V. Defects Are Needed for Fast Photo-Induced Electron Transfer from a Nanocrystal to a Molecule: Time-Domain Ab Initio Analysis. *J. Am. Chem. Soc.* **2013**, *135*, 18892−18900.
(87) Prezhdo, O. V.; Duncan, W. R.; Prezhdo, V. V. Photoinduced Electron Dynamics at the Chromophore−Semiconductor Interface: A Time-Domain Ab Initio Perspective. *Prog. Surf. Sci.* **2009**, *84*, 30−68.
(88) Kresse, G.; Furthmüller, J. Efficient Iterative Schemes for Ab Initio Total-Energy Calculations Using a Plane-Wave Basis Set. *Phys. Rev. B: Condens. Matter Mater. Phys.* **1996**, *54*, 11169−11186.
(89) Perdew, J. P.; Burke, K.; Ernzerhof, M. Generalized Gradient Approximation Made Simple. *Phys. Rev. Lett.* **1996**, *77*, 3865−3868.
(90) Blöchl, P. E. Projector Augmented-Wave Method. *Phys. Rev. B: Condens. Matter Mater. Phys.* **1994**, *50*, 17953−17979.
(91) Kohn, W.; Sham, L. J. Self-Consistent Equations Including Exchange and Correlation Effects. *Phys. Rev.* **1965**, *140*, A1133−A1138.
(92) Ivanov, D. S.; Zhigilei, L. V. Combined Atomistic-Continuum Modeling of Short-Pulse Laser Melting and Disintegration of Metal Films. *Phys. Rev. B: Condens. Matter Mater. Phys.* **2003**, *68*, 064114.
(93) Chen, X.; Prezhdo, O. V.; Ma, Z. Y.; Hou, T. J.; Guo, Z. Y.; Li, Y. Y. Ab Initio Phonon-Coupled Nonadiabatic Relaxation Dynamics of $Au_{25}(SH)_{18}^-$ Clusters. *Phys. Status Solidi B* **2016**, *253*, 458−462.
(94) Ranasingha, O.; Wang, H.; Zobac, V.; Jelinek, P.; Panapitiya, G.; Neukirch, A. J.; Prezhdo, O. V.; Lewis, J. P. Slow Relaxation of Surface Plasmon Excitations in Au-55: The Key to Efficient Plasmonic Heating in Au/TiO_2. *J. Phys. Chem. Lett.* **2016**, *7*, 1563−1569.
(95) Neukirch, A. J.; Guo, Z. Y.; Prezhdo, O. V. Time-Domain Ab Initio Study of Phonon-Induced Relaxation of Plasmon Excitations in a Silver Quantum Dot. *J. Phys. Chem. C* **2012**, *116*, 15034−15040.
(96) Habenicht, B. F.; Kamisaka, H.; Yamashita, K.; Prezhdo, O. V. Ab Initio Study of Vibrational Dephasing of Electronic Excitations in Semiconducting Carbon Nanotubes. *Nano Lett.* **2007**, *7*, 3260−3265.
(97) Kamisaka, H.; Kilina, S. V.; Yamashita, K.; Prezhdo, O. V. Ab Initio Study of Temperature- and Pressure Dependence of Energy and Phonon-Induced Dephasing of Electronic Excitations in Cdse and Pbse Quantum Dots. *J. Phys. Chem. C* **2008**, *112*, 7800−7808.
(98) Guo, Z. Y.; Habenicht, B. F.; Liang, W. Z.; Prezhdo, O. V. Ab Initio Study of Phonon-Induced Dephasing of Plasmon Excitations in Silver Quantum Dots. *Phys. Rev. B: Condens. Matter Mater. Phys.* **2010**, *81*, 10.1103/PhysRevB.81.125415.
(99) Liu, J.; Kilina, S. V.; Tretiak, S.; Prezhdo, O. V. Ligands Slow Down Pure-Dephasing in Semiconductor Quantum Dots. *ACS Nano* **2015**, *9*, 9106−9116.
(100) Pal, S.; Nijjar, P.; Frauenheim, T.; Prezhdo, O. V. Atomistic Analysis of Room Temperature Quantum Coherence in Two-Dimensional CdSe Nanostructures. *Nano Lett.* **2017**, *17*, 2389−2396.
(101) Tanimura, Y.; Mukamel, S. 2-Dimensional Femtosecond Vibrational Spectroscopy of Liquids. *J. Chem. Phys.* **1993**, *99*, 9496−9511.
(102) Fleming, G. R.; Cho, M. H. Chromophore-Solvent Dynamics. *Annu. Rev. Phys. Chem.* **1996**, *47*, 109−134.
(103) Miller, S. A.; Womick, J. M.; Parker, J. F.; Murray, R. W.; Moran, A. M. Femtosecond Relaxation Dynamics of $Au_{25}l_{18}$− Monolayer-Protected Clusters. *J. Phys. Chem. C* **2009**, *113*, 9440−9444.
(104) Yamaguchi, S.; Tahara, T. Coherence Acoustic Phonons in a Thin Gold Film Probed by Femtosecond Surface Plasmon Resonance. *J. Raman Spectrosc.* **2008**, *39*, 1703−1706.

DOI: 10.1021/acs.jpcc.7b05211
J. Phys. Chem. C 2017, 121, 17488−17497

(105) Lynn, J. W.; Smith, H. G.; Nicklow, R. M. Lattice Dynamics of Gold. *Phys. Rev. B* **1973**, *8*, 3493−3499.

DOI: 10.1021/acs.jpcc.7b05211
J. Phys. Chem. C 2017, 121, 17488−17497